Shock Waves (1998) 8: 127–137

(B - 38

Shock Waves

Numerical investigation of the propagation of shock waves in rigid* porous materials: flow field behavior and parametric study

A. Levy[1], G. Ben-Dor[1], S. Sorek[2]

[1] Pearlstone Center for Aeronautical Engineering Studies, Department of Mechanical Engineering, Ben-Gurion University of the Negev, Beer Sheva, Israel
[2] Water Resource Center, J. Blaustein Desert Research Institute, Ben-Gurion University of the Negev, Sede Boker Campus, Israel

Received 22 April 1996 / Accepted 5 January 1997

Abstract. A numerical parametric study of the flow field which develops when a planar shock wave impinge on a rigid porous material is presented. This study complements an earlier study (Levy et al. 1996a) where the values of some dominating parameters were estimated and the dependence of the resulting flow field on these values was not checked.

Key words: Shock wave, Compaction waves, Porous media, Cellular media

1 Introduction

A detailed investigation of the head-on collision of planar shock waves with rigid porous materials was initiated on the theoretical basis of macroscopic balance equations. The governing equations of macroscopic mass, momentum and energy balance, for a saturated porous medium, were developed by Levy et al. (1995) by conducting a dimensional analysis on the macroscopic balance equations of Bear et al. (1992) and Sorek et al. (1992). It was novel in establishing the macroscopic theoretical basis for nonlinear wave motion in multi-phase deformable porous media. The modeling was based on conceptualization of the porous medium as a continuum composed of interacting compressible solid and fluid phases (saturated porous media). Macroscopic physical laws expressing the mass, the momentum and the energy balances for the fluid phase and the solid matrix were formulated on the basis of Representative Elementary Volume (REV) concepts, presented by Bear and Bachmat (1990). These macroscopic balance equations were composed of averaged flux terms together with integrals of microscopic exchange flux terms at the solid/fluid interface. Some macroscopic parameters which resulted from the averaging process were the tortuosity factor which represents a tensor associated with the matrix directional cosines, the hydraulic radius of the pore spaces and the porosity which represents the volume fraction of the pores filled with the fluid. Note that unlike models developed in the past (e.g., Baer 1988), which accounted only for the properties of the phases, the macroscopic model developed in the course of study by Levy et al. (1995) also accounted for geometrical properties. Hence, in addition, the speed of the wave was also a function of the porous material structure. Unlike Bear and Bachmat (1990), Levy et al. (1995) showed that a Forchheimer term should be included as an additional macroscopic inertia term commencing from the microscopic inertia exchange between the phases at the solid/fluid interface.

A dimensional analysis was applied to the macroscopic balance equations of the phases after the simultaneous onset of an abrupt change of the pressure and temperature of the fluid. Levy et al. (1995) obtained four significant evolution periods. In the first evolution period, the pressure, the temperature and the stress were spatially distributed without attenuation. The vertical stress, however, depended linearly on the gravity. In the second evolution period, they noted that the momentum balance equations conform to nonlinear wave equations. In the third evolution period, the averaged inertial and dissipation terms were found to be of the same order of magnitude and consequently, the entire macroscopic Navier-Stokes equations should be considered. In the fourth evolution period, the inertial terms were found to be negligible in comparison with the dissipation terms. Assuming that the friction between the solid and the fluid was higher than the one between the fluid layers, the nonlinear Darcy law (including the Forchheimer term) for the momentum balance equation of the fluid was obtained.

Correspondence to: G. Ben-Dor

* We use the term "rigid" in the loose relative sense which is in common when applied to porous materials, in general, and in particular, i.e., that deformations do not exceed a few percent.

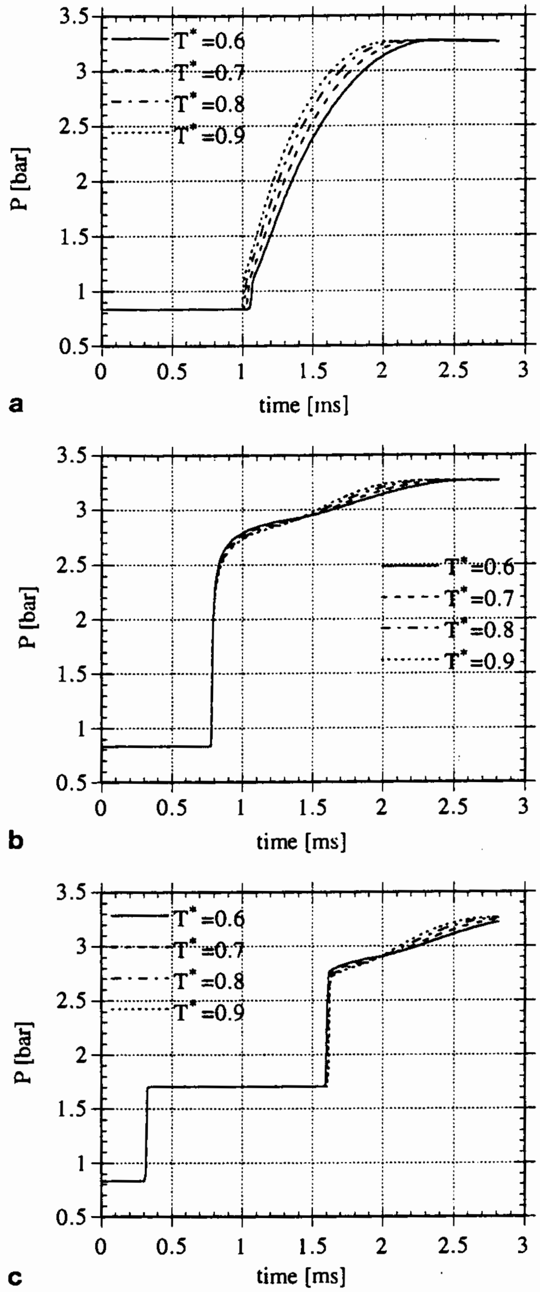

Fig. 1a–c. The dependence of the pressure field on the tortuosity: **a** at the back edge of the sample; **b** at the front edge of the sample; and **c** 42 cm ahead of the sample. The sample was made of silicon carbide and it was 81 mm long. The incident shock wave Mach number was M_i=1.377

In a following study, Levy et al. (1996b) developed a macroscopic one-dimensional analytical model for describing compression (shock) waves propagation in rigid porous media. Unlike Krylov et al. (1996) and Sorek et al. (1996) who neglected the momentum and the energy exchanges between the two phases at the solid/fluid interface and assumed that the coupling between them was only due to the effective stress, in Levy et al. (1996b) the momentum and the energy exchanges between the two phases were also accounted for. Based on the dimensional analysis of Levy et al. (1996a), it was shown that the linear Darcy term was much smaller than the nonlinear Forchheimer term. Consequently, only the latter appeared in the momentum and the energy exchanges between the two phases. In addition, it was assumed by Levy et al. (1996b) that both the porosity and the temperature of the solid phase remained constant and that the inertial force of the solid phase was negligibly small.

As part of the investigation, it was decided to solve numerically the full one-dimensional set of the governing equations as developed and presented by Levy et al. (1995). Since the full derivation of the governing equations can be found in Levy et al. (1995, 1996a) only the assumptions used in their derivation as well as their final form is given in the following. Levy et al. (1996a) also derived a TVD based computer code for solving the governing equations, Predictions, based on their code, were compared to the experimental results of Levy et al. (1993) and very good to excellent agreement was evident. Many more details can be found in Levy et al. (1996a).

2 Present study

2.1 The assumptions

1) The fluid is ideal (i.e., μ_f=0 and λ_f=0 where μ_f is the dynamic viscosity and λ_f is the thermal conductivity).
2) The fluid is a perfect gas.
3) The dispersive and diffusive mass fluxes of the fluid, and the dispersive flux of the solid, are much smaller than the corresponding advective ones and may, therefore, be neglected.
4) The dispersive momentum flux is much smaller than its advective one and may, therefore, be neglected.
5) The conductive and dispersive heat fluxes of the phases are negligibly small when compared to their advective ones.
6) The microscopic solid/fluid interface is a material surface with respect to the mass of both phases.
7) The solid matrix is thermoelastic, and is assumed to undergo small deformations only.
8) The stress-strain relationship for the solid, at the microscopic level, and for the solid matrix, at the macroscopic level, have the same form.
9) The material of which the skeleton of the porous material is made is incompressible.
10) The specific heats at constant volume, C_f , and that at constant strain, C_s, for the solid, are constant.
11) The energy processes for the fluid and for the solid are reversible.
12) There are no external energy sources.
13) The energy associated with the viscous dissipation is negligibly small.
14) The rate of heat transferred between the fluid and the solid phases is negligibly small.

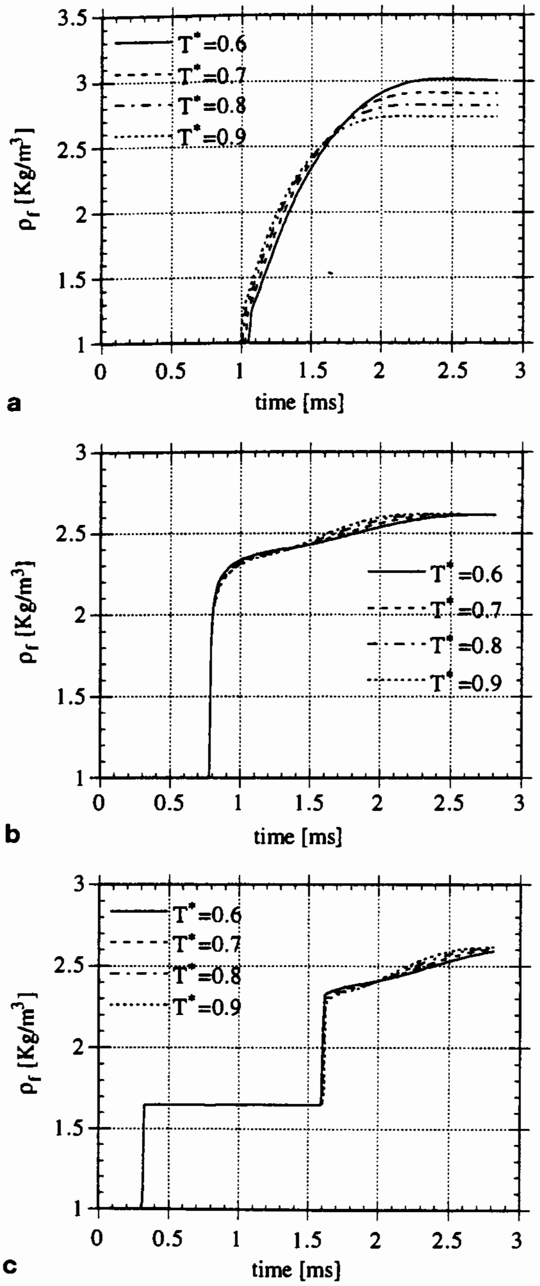

Fig. 2a–c. The dependence of the fluid density field on the tortuosity: **a** at the back edge of the sample; **b** at the front edge of the sample; and **c** 42 cm ahead of the sample. The sample was made of silicon carbide and it was 81 mm long. The incident shock wave Mach number was M_i=1.377

2.2 The balance equations

The macroscopic mass balance equation for the fluid phase is:

$$\frac{\partial \phi \rho_f}{\partial t} = -\nabla \cdot \phi \rho_f \mathbf{V}_f, \tag{1}$$

where ρ_f is the density of the fluid, $\mathbf{V}_f$ denotes its velocity vector and ϕ denotes porosity.

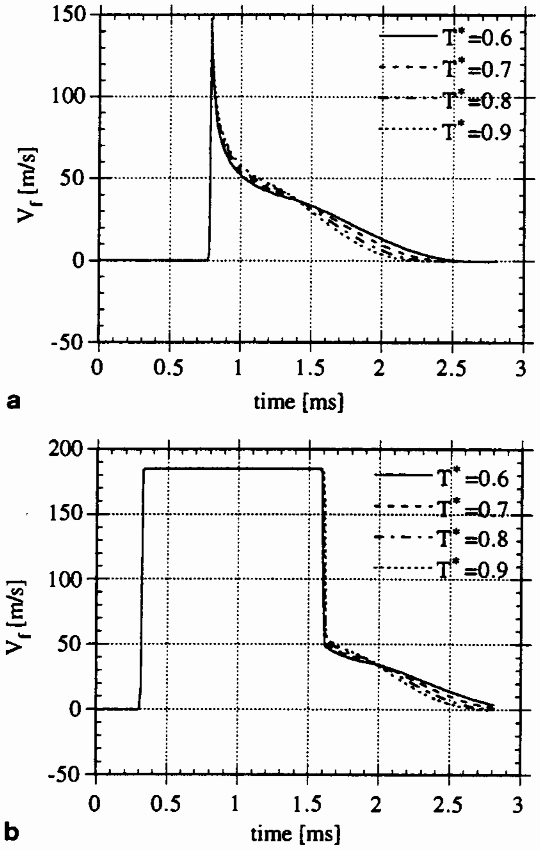

Fig. 3a,b. The dependence of the fluid velocity on the tortuosity: **a** at the front edge of the sample; and **b** 42 cm ahead of the sample. The sample was made of silicon carbide and it was 81 mm long. The incident shock wave Mach number was M_i=1.377

The macroscopic mass balance equation for the solid phase is:

$$\frac{\partial (1-\phi)\rho_s}{\partial t} = -\nabla \cdot (1-\phi)\rho_s \mathbf{V}_s, \tag{2}$$

where ρ_s is the density of the solid and $\mathbf{V}_s$ denotes its velocity vector.
The macroscopic momentum balance equation for the fluid phase is:

$$\begin{aligned}\frac{\partial \phi \rho_f \mathbf{V}_f}{\partial t} = & -\nabla \cdot \phi \rho_f \mathbf{V}_f \mathbf{V}_f \\ & -\phi \mathbf{T}^* \nabla P - \phi \rho_f g \mathbf{T}^* \nabla Z \\ & -\frac{c_f}{2\Delta_f^2} \tilde{\mathbf{F}} \phi \rho_f (\mathbf{V}_f - \mathbf{V}_s)(\mathbf{V}_f - \mathbf{V}_s),\end{aligned} \tag{3}$$

where P which denotes the pressure of the fluid is prescribed by the equation of state, see (7), g denotes the acceleration of gravity in the z direction, $\tilde{\mathbf{F}}$ and $\mathbf{T}^*$ denote the Forchheimer tensor for an isotropic solid matrix and the tortuosity tensor associated with the directional cosines at the solid/fluid interface, respectively, c_f denotes a shape factor and Δ_f denotes the hydraulic radius of the pore spaces.

The macroscopic momentum balance equation for the solid phase is:

$$\begin{aligned}\frac{\partial(1-\phi)\rho_s\mathbf{V}_s}{\partial t} &= -\nabla\cdot[(1-\phi)\rho_s\mathbf{V}_s\mathbf{V}_s] \\ &\quad -(1-\phi)\mathbf{T}_s^*\nabla P+\nabla\sigma_s' \\ &\quad +(1-\phi)\rho_s g\mathbf{T}^*\nabla Z \\ &\quad +\frac{c_f}{2\Delta_f^2}\tilde{\mathbf{F}}\phi\rho_f(\mathbf{V}_f-\mathbf{V}_s) \\ &\quad \times(\mathbf{V}_f-\mathbf{V}_s),\end{aligned} \tag{4}$$

where σ_s' denotes the macroscopic constitutive relation for the effective stress of a thermoelastic solid matrix as given Bear et al. (1992). It is expressed in Eq. (8).

The macroscopic energy balance equation for the fluid phase is:

$$\begin{aligned}&\frac{\partial}{\partial t}[\phi\rho_f(C_fT_f+\frac{\mathbf{V}_f^2}{2})] \\ &= -\nabla\cdot[\phi\rho_f\mathbf{V}_f(C_fT_f+\frac{\mathbf{V}_f^2}{2})] \\ &\quad -\mathbf{T}^*\nabla\phi P\mathbf{V}_f+\mathbf{T}^*P\mathbf{V}_s\nabla\phi \\ &\quad -\frac{c_f}{2\Delta_f^2}\tilde{\mathbf{F}}\phi\rho_f(\mathbf{V}_f-\mathbf{V}_s)(\mathbf{V}_f-\mathbf{V}_s)\mathbf{V}_s,\end{aligned} \tag{5}$$

where T_f and C_f are the temperature and the specific heat at constant volume of the fluid phase, respectively.

The macroscopic energy balance equation for the solid phase is:

$$\begin{aligned}&\frac{\partial}{\partial t}[(1-\phi)\rho_s(C_sT_s+\frac{\mathbf{V}_s^2}{2})] \\ &= -\nabla\cdot[(1-\phi)\rho_s\mathbf{V}_f(C_sT_s+\frac{\mathbf{V}_s^2}{2})] \\ &\quad +\nabla\sigma_s'\mathbf{V}_s-\mathbf{T}^*\nabla(1-\phi)P\mathbf{V}_s-\mathbf{T}^*P\mathbf{V}_s\nabla\phi \\ &\quad +\frac{c_f}{2\Delta_f^2}\tilde{\mathbf{F}}\phi\rho_f(\mathbf{V}_f-\mathbf{V}_s)(\mathbf{V}_f-\mathbf{V}_s)\mathbf{V}_s,\end{aligned} \tag{6}$$

where T_s and C_s are the temperature and the specific heat at constant strain of the solid phase, respectively.

The equation of state for the fluid phase is:

$$P=\rho_f\mathrm{R}T_f, \tag{7}$$

here R is the specific gas constant. The effective stress for a thermoelastic solid matrix, which is assumed to undergo small deformations only, is:

$$\sigma_s'=\lambda_s''\varepsilon_{skel}\mathbf{I}+\mu_S'\varepsilon_{skel}-\eta(T_s-T_{s0})\mathbf{I}, \tag{8}$$

where μ_s', λ_s'' and η denote the Lamé constants of a thermoelastic solid and $\mathbf{I}$ denotes the unit tensor. The macroscopic strain tensor for the solid matrix, ε_{skel}, is defined for small deformations by the compatibility law

$$\varepsilon_{skel}=\frac{1}{2}[\nabla\mathbf{w}_s+(\nabla\mathbf{w}_s)^T], \tag{9}$$

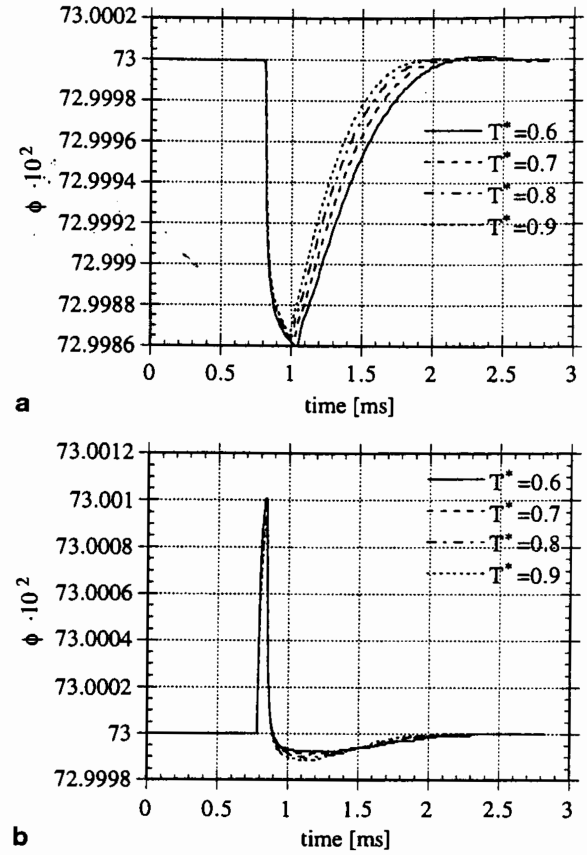

Fig. 4a,b. The dependence of the porosity on the tortuosity: **a** at the back edge of the sample; and **b** at the front edge of the sample. The sample was made of silicon carbide and it was 81 mm long. The incident shock wave Mach number was M_i=1.377

in which $\mathbf{w}_s$ denotes the displacement vector of the solid matrix. The volumetric strain ($\equiv$ dilatation), ε_{skel}, is given by

$$\varepsilon_{skel}=\nabla\cdot\mathbf{w}_s. \tag{10}$$

Combining (10) and (2) while recalling that ρ_s= constant results in

$$\nabla\cdot\mathbf{V}_s=\frac{1}{1-\phi}\frac{D_s\phi}{Dt}=\frac{D_s\varepsilon_{skel}}{Dt},$$

$$\frac{D_s(\,)}{Dt}\equiv\frac{\partial}{\partial t}(\,)+\mathbf{V}_s\cdot\nabla(\,), \tag{11}$$

in which the following definition has been used

$$\mathbf{V}_s\equiv\frac{D_s\mathbf{w}_s}{Dt}. \tag{12}$$

2.3 The one-dimensional governing equations

The one-dimensional version of the above set of governing equations, in a vector form, reads :

$$\frac{\partial\mathbf{U}}{\partial t}+\frac{\partial\mathbf{F}}{\partial x}=\mathbf{Q}. \tag{13}$$

The variables vector, $\mathbf{U}$, is defined by

$$\mathbf{U} = [r_f, r_s, m_f, m_s, E_f, E_s]^T, \tag{14}$$

where

$$r_f \equiv \phi\rho_f\ ,\ m_f \equiv r_f V_f\ ,\ r_s \equiv (1-\phi)\rho_s\ ,\ m_s \equiv r_s V_s,$$

$$E_f \equiv r_f e_f = r_f(C_f T_f + \frac{V_f^2}{2}),$$

$$E_s \equiv r_s e_s = r_s(C_s T_s + \frac{V_s^2}{2}). \tag{15}$$

The flux vector, $\mathbf{F}$, is

$$\mathbf{F} = \begin{pmatrix} m_f \\ m_s \\ \frac{m_f^2}{r_f} + T^*\phi P \\ \frac{m_s^2}{r_s} - \sigma_s^{'} + (1-\phi T^*)P \\ \frac{m_f}{r_f}(E_f + T^*\phi P) \\ \frac{m_s}{r_s}(E_s - \sigma_s^{'} + (1-\phi T^*)P) \end{pmatrix}. \tag{16}$$

The source vector, $\mathbf{Q}$, is

$$\mathbf{Q} = \begin{pmatrix} 0 \\ 0 \\ T^* P\frac{\partial\phi}{\partial x} - \tilde{F} r_f |\frac{m_f}{r_f} - \frac{m_s}{r_s}|(\frac{m_f}{r_f} - \frac{m_s}{r_s}) \\ -T^* P\frac{\partial\phi}{\partial x} + \tilde{F} r_f |\frac{m_f}{r_f} - \frac{m_s}{r_s}|(\frac{m_f}{r_f} - \frac{m_s}{r_s}) \\ \frac{m_s}{r_s}(T^* P\frac{\partial\phi}{\partial x} - \tilde{F} r_f |\frac{m_f}{r_f} - \frac{m_s}{r_s}|(\frac{m_f}{r_f} - \frac{m_s}{r_s})) \\ \frac{m_s}{r_s}(-T^* P\frac{\partial\phi}{\partial x} + \tilde{F} r_f |\frac{m_f}{r_f} - \frac{m_s}{r_s}|(\frac{m_f}{r_f} - \frac{m_s}{r_s})) \end{pmatrix} \tag{17}$$

where ϕP and $\sigma_s^{'}$ which appear in (16) are defined as follows:

$$\phi P = (\gamma - 1)[E_f - \frac{m_f^2}{2r_f}], \tag{18}$$

$$\sigma_s^{'} = E_\varepsilon \varepsilon - E_T C_s (T_s - T_{s0}). \tag{19}$$

In the above equations $E_\varepsilon (\equiv \lambda_s^{''} + \mu_s^{'})$ and $E_T (\equiv \eta / C_s)$ are the one-dimensional macroscopic Lamé coefficients for a thermoelastic solid. With the aid of definitions (15) the porosity, ϕ, can be written as,

$$\phi = 1 - \frac{r_S}{\rho_S}. \tag{20}$$

By solving (2) analytically and with the aid of (15) the strain can be expressed as a function of the porosity as,

$$\varepsilon = 1 - \frac{r_s}{r_{s0}}. \tag{21}$$

With the aid of (15), (19) can be rewritten as

$$\sigma_s^{'} = E_\varepsilon (\frac{r_{s0} - r_s}{r_{s0}}) - E_T (\frac{E_s}{r_s} - \frac{E_{s0}}{r_{s0}} - \frac{m_s^2}{2r_s^2} + \frac{m_{s0}^2}{2r_{s0}^2}). \tag{22}$$

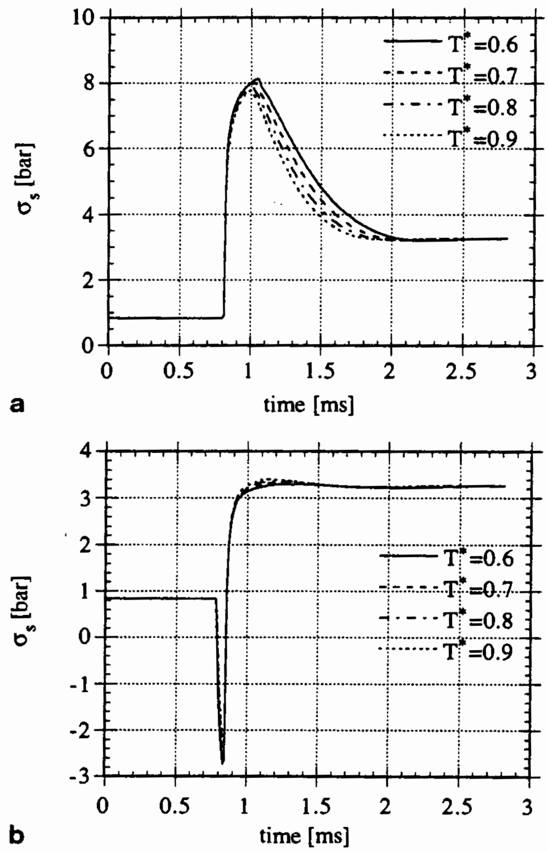

Fig. 5a,b. The dependence of the normal stress on the tortuosity: **a** at the back edge of the sample; and **b** at the front edge of the sample. The sample was made of silicon carbide and it was 81 mm long. The incident shock wave Mach number was M_i=1.377

The above set of equations consists of six differential equations, described by (13) and (14), and six unknowns namely: r_f, r_s, m_f, m_s, E_f and E_s. Consequently, in principle, the equations are complete and can therefore be solved. Due to the complexity of the equations, an analytical solution is impossible. A reliable TVD based numerical code for solving these equations was developed by Levy et al. (1996a). It should be noted, however, that simplified cases were solved analytically by Krylov et al. (1996) and Sorek et al. (1996).

As mentioned above, numerical predictions based on a TVD based computer code which was developed by Levy et al. (1996a) very well to excellently agreed with the experimental results of Levy et al. (1993). Consequently, it was believed that the analytical model and the numerical code were reliable enough to conduct a parametric study of the flow field under investigation. This parametric investigation is presented in the following.

As shown in Levy et al. (1996a) the solution of the governing equations required the knowledge of the following parameters: the macroscopic Lamé coefficients for a thermoelastic solid, E_ε and E_T, the Forchheimer factor, $\tilde{F}$, the tortuosity, T^*, the initial porosity, ϕ_0, and the density of the solid matrix, ρ_s. Out of these six parameters

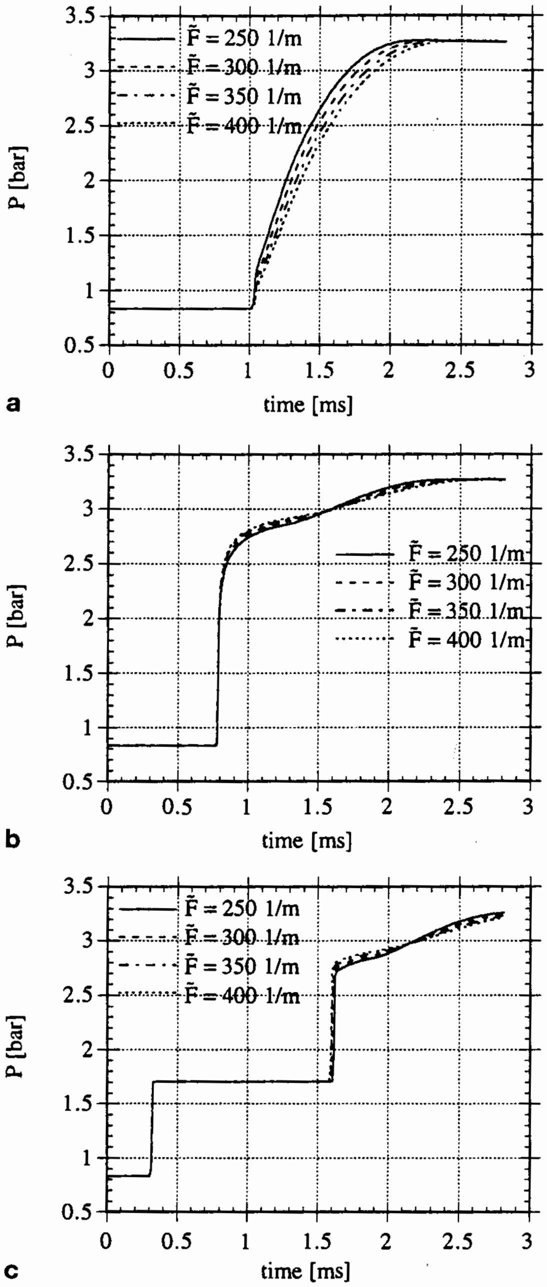

Fig. 6a–c. The dependence of the pressure field on the Forchheimer factor: **a** at the back edge of the sample; **b** at the front edge of the sample; and **c** 42 cm ahead of the sample. The sample was made of silicon carbide and it was 81 mm long. The incident shock wave Mach number was M_i=1.377

only one, namely the density of the solid matrix, ρ_s, was available from the manufacturer. The other five parameters had to be estimated. Levy et al. (1993) calculated the porosity using (20) which is limited to gas saturated porous materials, in which r_s is, in fact, the bulk density of the porous material. Its value was obtained by dividing the mass of a given sample by its volume and ρ_s, as mentioned earlier, was provided by the manufacturer. The porosity value as obtained and reported by Levy et al. (1993) was 0.728±0.016.

Table 1. The initial porosity, the tortuosity and the Forchheimer factors for the different samples

The Sample Material	Sample Type	Pores per Inch (ppi)	Initial Porosity	$\tilde{F}$ [1/m]	T^*
Silicon Carbide[1]	I	10	0.728±0.016	300	0.7
(SiC)	II	20	0.745±0.001	500	0.7
Alumina[1]	III	30	0.814±0.010	900	0.75
(Al_2O_3)	IV	40	0.821±0.007	1800	0.75

1. The structure of the porous material was open cell

Based on the properties of the materials of which the samples were made, and the fact that the upper limit of the elastic stress reduces when the porosity increases, in a $(1-\phi)^2$ manner, see Gibson and Ashby (1988), the orders of magnitude of the macroscopic Lamé coefficients which appear in the macroscopic constitutive equation for thermoelastic porous materials, E_ε and E_T were estimated to be identical for all the samples which were used in the course of the experimental study: $E_\varepsilon = 380 \times 10^7$ Pa; and $E_T = 26.207$ kg/m^3. The tortuosity factors, T^*, is a geometric parameter which accounts for the fact that the average pressure gradient and the average fluid velocity are not parallel. The tortuosity in gases is, in general, smaller than unity. It was found, for the various samples, by estimating the ratio between the speed of sound of the air inside the porous medium, a^*, and that in a pure air, a, with the aid of the following relation:

$$T^{2*} + \frac{1}{\gamma-1}T^* - \frac{\gamma}{\gamma-1}\left(\frac{a^*}{a}\right)^2 = 0, \qquad (23)$$

where γ is its specific heat capacities ratio. Li et al. (1995) estimated the value of a^* by using the experimental results of Levy et al. (1993).

The Forchheimer factors, $\tilde{F}$, for the various samples were found experimentally. In these experiments, each sample was mounted in a pipe and the pressure drop across it was measured as a function of the air flow rate through it. The pressure drop was found to be a parabolic function of the air velocity. This was done by assuming that the pressure drop depended linearly on the length of the sample. The values of the tortuosity and the Forchheimer factors, as obtained experimentally for the various samples, used in the present study, are presented in Table 1.

3 The parametric study

Prior to presenting the parametric study it is important to draw the reader's attention to the footnote on the first page. Both the analytical model and the numerical code were developed for a thermoelastic porous material, i.e., the material is not totally rigid. Had it been totally rigid another analytical model and numerical code would have been obtained. The solid matrix as well as the process taking place inside it would have been cancelled out all together.

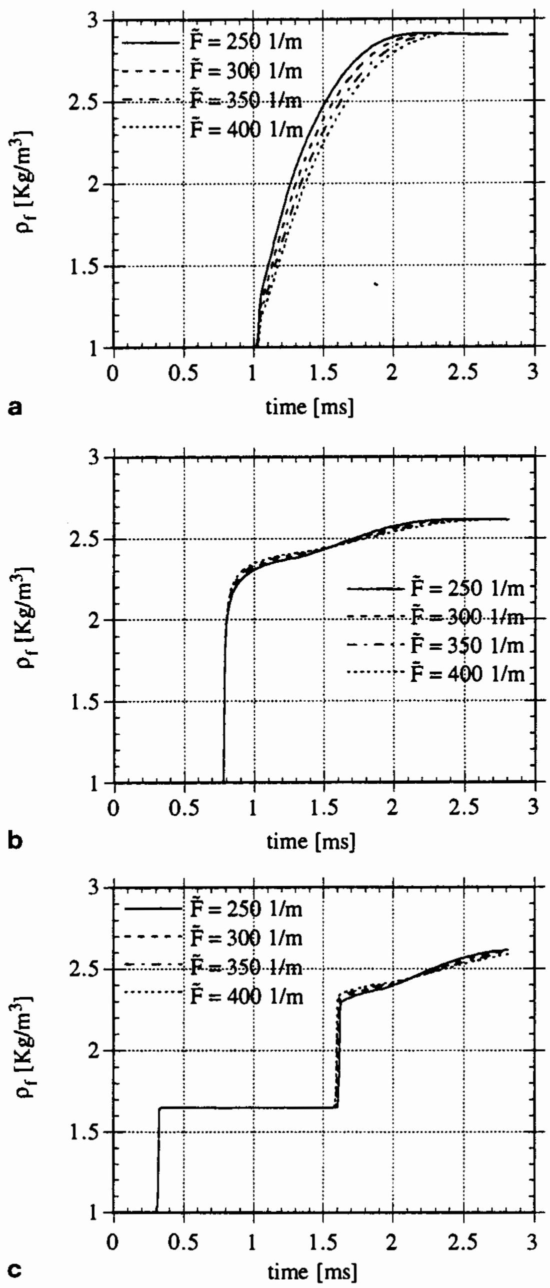

Fig. 7a–c. The dependence of the fluid density field on the Forchheimer factor: **a** at the back edge of the sample; **b** at the front edge of the sample; and **c** 42 cm ahead of the sample. The sample was made of silicon carbide and it was 81 mm long. The incident shock wave Mach number was M_i=1.377

In addition, ignoring the effect of elasticity would result in a situation in which the overall phenomenon would be misunderstood. For this reason investigating the influence of the various parameters on the porosity, the solid velocity and the normal stress are important.

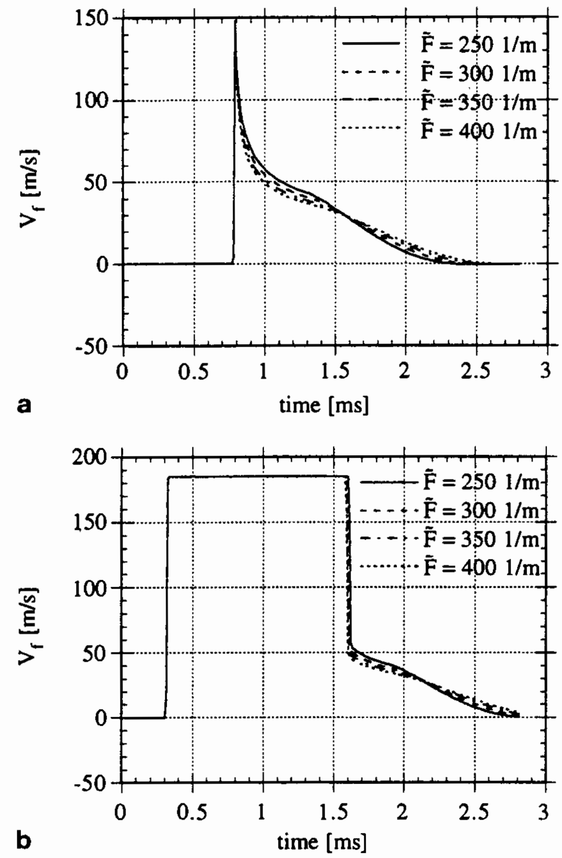

Fig. 8a,b. The dependence of the fluid velocity on the Forchheimer factor: **a** at the front edge of the sample; and **b** 42 cm ahead of the sample. The sample was made of silicon carbide and it was 81 mm long. The incident shock wave Mach number was M_i=1.377

3.1 The tortuosity effect

The dependence of the pressure field on the tortuosity is shown in Figs. 1a to 1c for an 81 mm long sample of silicon carbide (SiC) struck head-on by an incident shock wave having a Mach number M_i=1.377. The pressure profile at the back edge of the sample is shown in Fig. 1a, the pressure profile at the front edge of the sample is shown in Fig. 1b, and the pressure profile 42 cm ahead of the sample is shown in Fig. 1c.

It is evident from Fig. 1a that the compression (shock) wave velocity increases as the tortuosity increases. Note that the compression (shock) wave reaches the back edge of the sample about 75 μsec earlier for $T^* = 0.9$ as compared to $T^* = 0.6$. Figures 1a to 1c also indicate that while the tortuosity has a meaningful influence on the pressure at the back edge of the sample (Fig. 1a), its effect at the front edge is less significant (Fig. 1b). As shown in Fig. 1c, the tortuosity has an effect on the pressure also, in the pure gas, ahead if the sample. It is evident from Fig. 1c that the reflected shock wave moves faster when the tortuosity is smaller.

Figure 1a also indicates that the pressure rise depends on the tortuosity (it is faster when the tortuosity is larger). This fact implies that the impulse, $\int Pdt$, is larger for

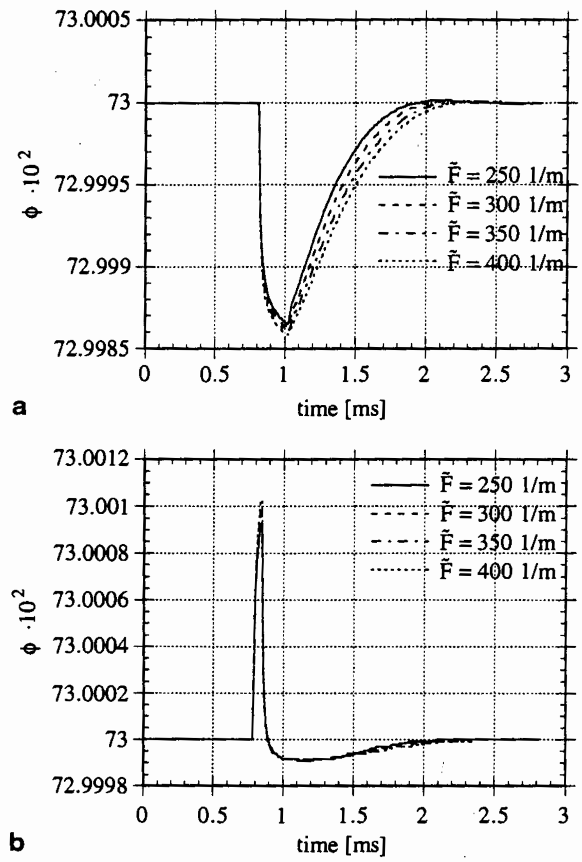

Fig. 9a,b. The dependence of the porosity on the Forchheimer factor: **a** at the back edge of the sample; and **b** at the front edge of the sample. The sample was made of silicon carbide and it was 81

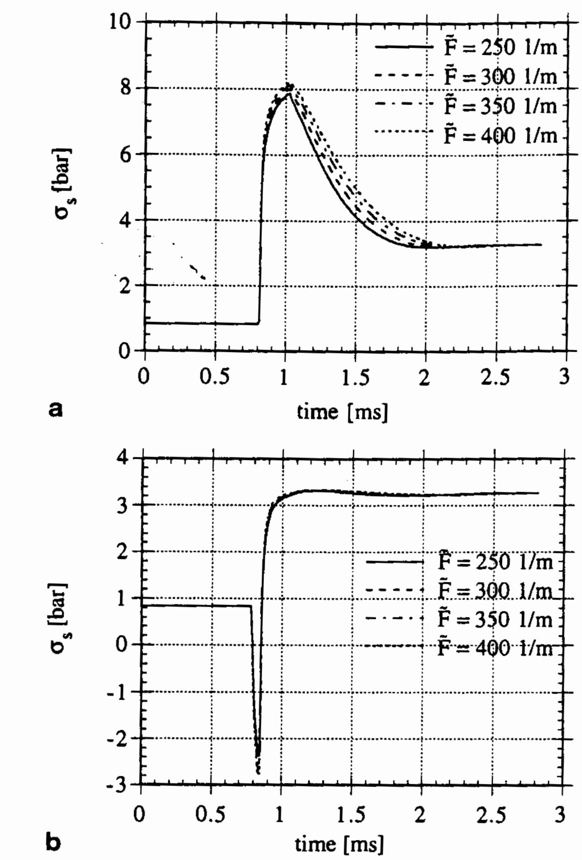

Fig. 10a,b. The dependence of the normal stress on the Forchheimer factor: **a** at the back edge of the sample; and **b** at the front edge of the sample. The sample was made of silicon carbide and it

higher tortuosities. The finally obtained pressure, however, is independent of the tortuosity. The situation is similar when the pressure at the front edge of the sample is considered (see Fig. 1b). However Fig. 1c indicates that the finally obtained pressure ahead of the sample does depend on the tortuosity. It is seen to reach higher values for larger tortuosities. It should be noted here, however, that if the computation was allowed to proceed further in time a situation in which the finally obtained pressures ahead of the sample also approach each other could have been obtained.

The effect of the tortuosity on the fluid density is shown in Figs. 2a to 2c. Again a significant influence is shown at the back edge of the sample, and smaller influences are evident at the front edge and ahead of the sample. Unlike Fig. 1a where the same final pressures were obtained at the back edge, the final densities at the back edge are different. They are higher for smaller tortuosities. While for $T^* = 0.9$, ρ_f reaches a value of about 2.7 kg/m^3, for $T^* = 0.6$ ρ_f increases by about 10% and reaches a value of about 3 kg/m^3.

The dependence of the fluid velocity, V_f, at the front edge and ahead of the sample on the tortuosity is shown in Figs. 3a and 3b, respectively. While the velocity flow field distribution shows a dependence on the tortuosity, the finally reached values are independent of the tortuosity at the front edge (Fig. 3a). When the velocity flow field ahead of sample is considered (Fig. 3b), a dependence of the finally reached values on the tortuosity is evident. The finally reached velocity is larger for smaller tortuosities. Our earlier note regarding longer computation times should be repeated here.

The dependence of the porosity, ϕ, on the tortuosity at the back and the front edges of the sample is shown in Figs. 4a and 4b, respectively. It is evident from these figures that the influence of the tortuosity on the porosity is more enhanced at the back edge. However, in view of the very small changes in the ϕ-axis, the porosity could be assumed to be constant and independent of the tortuosity. It is important to note here that two waves are transmitted into the porous material when the incident shock wave strikes it. The first is a very rapid compaction wave which propagates in the solid matrix, and the second is a compression (shock) wave which propagates through the gaseous phase occupying the pores. These waves interact at the solid/fluid interface inside the porous material. The compaction wave, which is very fast, is responsible for the fast porosity changes. It is difficult to illustrate the propagation time (from the front edge to the back edge) of the compaction wave on the time scale of Fig. 4. A descriptio

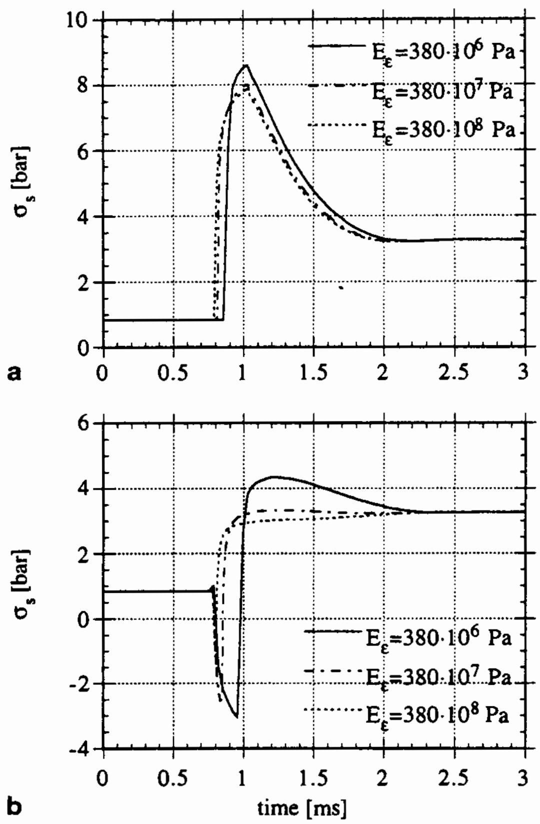

Fig. 11a,b. The dependence of the normal stress on the Lamé coefficient, E_ε: **a** at the back edge of the sample; and **b** at the front edge of the sample. The sample was made of silicon carbide and it was 81 mm long. The incident shock wave Mach number was $M_i = 1.377$

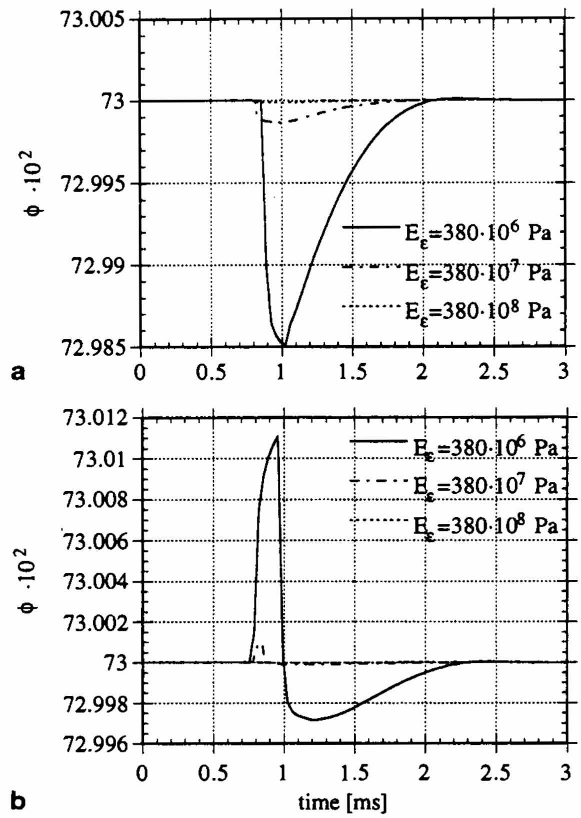

Fig. 12a,b. The dependence of the porosity on the Lamé coefficient, E_ε: **a** at the back edge of the sample; and **b** at the front edge of the sample. The sample was made of silicon carbide and it was 81 mm long. The incident shock wave Mach number was $M_i = 1.377$

of the waves system inside the porous medium and the influence of both the compression and the compaction waves on the porosity and the propagation time is presented in Levy et al. (1997).

Although not shown here, the solid matrix velocity, V_s, was found to be practically independent of the tortuosity, T^*.

The dependence of the normal stress, σ_s, at the back and the front edges of the sample on the tortuosity is shown in Figs. 5a and 5b, respectively. Again a more significant influence is evident at the back edge. It is evident from Fig. 6a that smaller tortuosities result in larger stresses. In analogy to the earlier note about the impulse, it is evident from Fig. 6a that $\int \sigma dt$ is larger for smaller tortuosities. However, long times after the initiation of the interaction all the profiles converge to a single line and the finally obtained normal stresses are independent of the tortuosity. Figure 5b reveals that the normal stress at the front edge of the sample is practically independent of the tortuosity.

3.2 The Forchheimer factor effect

The dependence of the pressure field on the Forchheimer factor is shown in Figs. 6a to 6c for an 81 mm long sample of SiC struck head-on by an incident shock wave having a Mach number $M_i = 1.377$. The pressure profile at the back edge of the sample is shown in Fig. 6a, the pressure profile at the front edge of the sample is shown in Fig. 6b, and the pressure profile 42 cm ahead of the sample is shown in Fig. 6c.

Figure 6a indicates that the compression (shock) wave velocity is not influenced by the Forchheimer factor as the profiles for the various Forchheimer factors start to rise at the same time. The finally obtained pressure is also seen to be independent of the Forchheimer factor. However, the pressure rises faster for smaller Forchheimer factors. Consequently, the impulse, $\int Pdt$, increases as the Forchheimer factor decreases. As can be seen in Figs. 6b and 6c the pressures at the front edge of the sample and ahead of it are less influenced by the Forchheimer factor.

The dependence of the fluid density profiles on the Forchheimer factor at the back edge, the front edge, and ahead of the sample, is shown in Figs. 7a to 7c, respectively. It is again evident from these figures that the most significant influence is at the back edge where the density is seen to rise faster for smaller Forchheimer factors. At the front edge and ahead of the sample, the effect of the Forchheimer factor on the fluid density profile is minor, and so is its effect ahead of the sample (see Figs. 7b and 7c, respectively).

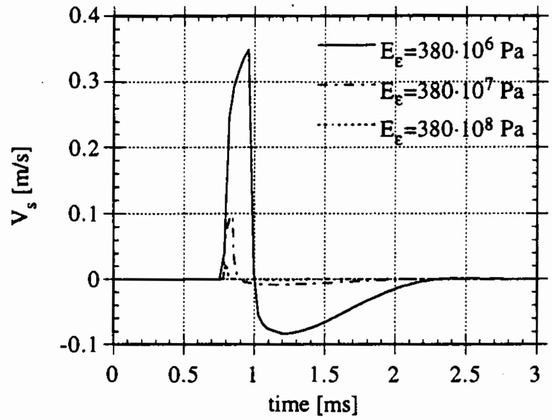

Fig. 13. The dependence of the solid matrix velocity on the Lamé coefficient, E_ε, at the front edge of the sample. The sample was made of silicon carbide and it was 81 mm long. The incident shock wave Mach number was M_i=1.377

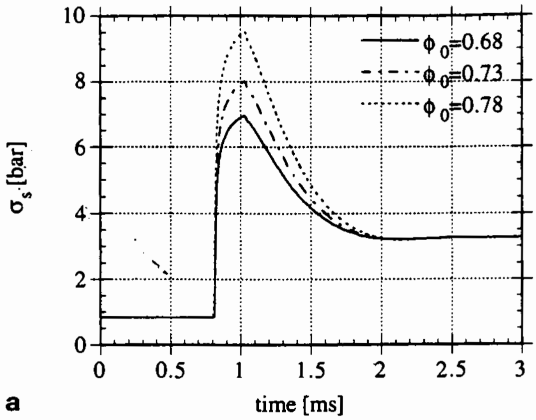

a

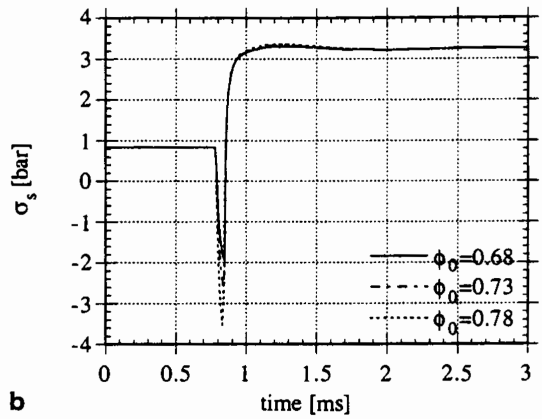

b

Fig. 14a,b. The dependence of the normal stress on the initial porosity: **a** at the back edge of the sample; and **b** at the front edge of the sample. The sample was made of silicon carbide and it was 81 mm long. The incident shock wave Mach number was M_i=1.377

The dependence of the fluid velocity, V_f, at the front edge and 42 cm ahead of the sample on the Forchheimer factor is shown in Figs. 8a and 8b, respectively. It is evident from these Figs. that differences of up to 7 m/s are obtained for different Forchheimer factors (e.g., at about 1 ms and 2 ms in Fig. 8a). However, the finally obtained fluid velocities are independent of the Forchheimer factor. It is also of interest to note that at about 1.6 ms after the interaction started, all the fluid velocity profiles converge to a single value (see 1.6 ms in Fig. 8a). A similar behavior is observed ahead of the sample (Fig. 8b at 2.1 ms). The reason for these findings is yet to be understood.

The dependence of the porosity, ϕ, on the Forchheimer factor at the back and the front edges of the sample is shown in Figs. 9a and 9b, respectively. While a more significant influence is evident at the back edge of the sample, it should be noted that owing to the fact that the incident shock wave is not too strong the porosity is practically constant (note the scale of the ϕ-axis). The solid matrix velocity, V_s, was found to be practically independent of the Forchheimer factor.

The dependence of the normal stress, σ_s, at the back and the front edges of the sample on the Forchheimer factor is shown in Figs. 10a and 10b, respectively. Again a more significant influence is evident at the back edge. It is evident from Fig. 10a that larger Forchheimer factors result in larger stresses and as a result larger "impulses" $\int \sigma dt$. At about 1.5 ms after the interaction the normal stress at the back edge of the sample is about 5 kPa for $\tilde{T}$ = 400 1/m and 20% less, i.e., about 4 kPa for $\tilde{T}$ = 250 1/m. Note that the finally obtained values of the normal stress are constant and independent of the Forchheimer factor.

3.3 The Lamé coefficients effect

The Lamé coefficients as chosen by Levy et al. (1996a) where $E_\varepsilon = 380 \times 10^7$ Pa and $E_T = 26.207$ kg/m^3. In order to check their influence on the resulted flow field, their values were first decreased and then increased by a factor of 10. No noticeable influence of E_T on the numerical results was obtained. E_ε was also found to have no influence on the pressure, the fluid density and the fluid velocity. Although the largest E_ε was two orders of magnitude greater than the smallest one, the resulted profiles were almost identical, and the times of arrival of the reflected shock waves were also the same. E_ε does have, however, a more significant influence on the normal stress profiles, σ_s, as can be seen in Figs. 11a and 11b, where the profiles of the normalized stress at the back and the front edges of the sample are, respectively, shown. The normal stresses are seen to reach higher values for the smallest value of E_ε. In addition, the finally obtained values of the normal stress are constant and they are independent of E_ε. It should also be noted that the compression (shock) wave reaches the rear edge of the sample faster for larger values of E_ε. The difference in the time of arrival between $E_\varepsilon = 380 \times 10^8$ Pa and $E_\varepsilon = 380 \times 10^6$ Pa is about 90 μs.

The dependence of the porosity on E_ε at the back and the front edges of the sample is shown in Figs. 12a and 12b, respectively. For the largest E_ε the porosity seems to be constant both at the back and at the front edges. As E_ε decreases the porosity is seen to depend more and more on E_ε. However. one should recall our earlier remark about

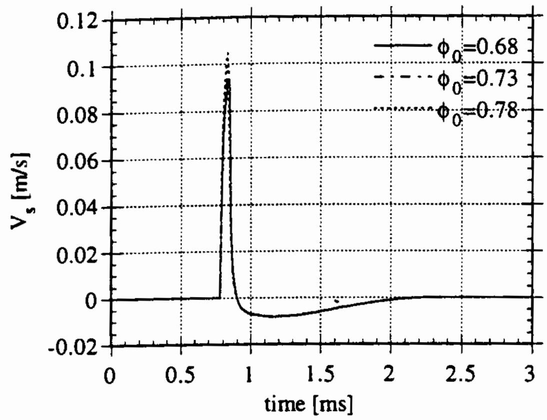

Fig. 15. The dependence of the solid matrix velocity on the initial porosity at the front edge of the sample. The sample was made of silicon carbide and it was 81 mm long. The incident shock wave Mach number was M_i=1.377

the scale of the ϕ-axis from which it is quite clear that, for moderate incident shock waves, the porosity, practically does not depend on E_ε.

The dependence of the solid matrix velocity, V_s, on E_ε at the front edge of the sample is shown in Fig. 13. Larger velocities are obtained for smaller values of E_ε. While for $E_\varepsilon = 380 \times 10^8$ Pa the largest solid matrix velocity is about 0.02 m/s, it is about 0.1 m/s for $E_\varepsilon = 380 \times 10^7$ Pa, and about 0.34 m/s for $E_\varepsilon = 380 \times 10^6$ Pa.

3.4 The initial porosity effect

The dependence of the pressure profiles at the back edge, at the front edge and ahead of the sample on the initial porosity, ϕ_0, was found to be extremely minor. Similar negligibly small dependence of the fluid density and the fluid velocity on ϕ_0, were also evident in the course of the numerical investigation.

A significant dependence on the initial porosity, ϕ_0, is exhibited in Figs. 14a and 14b where the normal stress profiles at the back and the front edges of the sample are shown. The larger is the porosity the higher is the normal stress and its "impulse". For example Fig. 14a indicates that for $\phi_0 = 0.68 (\sigma_s)_{\max} \approx 6.9$ kPa while for $\phi_0 = 0.78 (\sigma_s)_{\max} \approx 9.5$ kPa.

The influence of ϕ_0 on the solid matrix velocity, V_s, is shown in Fig. 15. It is evident that an increase from 0.68 to 0.78 in ϕ_0 results in a meaningful increase of about 14% in V_s from about 0.092 m/s to about 0.105 m/s.

4 Conclusions

A numerical solution of the flow field which results when a planar shock wave strikes head-on a rigid porous material was presented by Levy et al. (1996a). Their solution, required the estimation of the tortuosity, the Forchheimer factor, the Lamé coefficients and the initial porosity.

Owing to the fact that predictions based on their analytical model and numerical code were found to well agree with experimental results, the code was used to numerically investigate the influence of the above mentioned parameters on the obtained flow field.

The dependence of the pressure, the fluid density, the fluid velocity, the porosity, the normal stress and the solid matrix velocity on these parameters was investigated and studied, here.

As a result of the present study the investigated phenomenon which caught the attention of many investigators in the past decade is clearer and better understood.

References

Baer MR (1988) Numerical studies of dynamic compaction of inert and energetic granular materials. ASME J of Applied Mech 55: 36–43

Bear J, Bachmat Y (1990) Introduction to Modeling of Transport Phenomena in Porous Media. Kluwer Academic Publishers, Dordrecht, The Netherlands

Bear J, Sorek S, Ben-Dor G , Mazor G (1992) Displacement waves in saturated thermoelastic porous media. Part I. Basic equations. Fluid Dynamic Research 9: 155–164

Gibson LJ, Ashby MF (1988) Cellular Solids - Structure and Properties. Program Press, Hill Hall, Oxford, England

Krylov A, Sorek S, Levy A, Ben-Dor G (1996) Simple waves in saturated porous media.Part I. The isothermal case. Japan Society of Mech Eng Int J B 39: 294–298

Levy A (1995) Wave Propagation in a Saturated Porous Media. Ph.D Thesis. Department of Mechanical Engineering, Ben-Gurion University of the Negev, Beer Sheva, Israel

Levy A, Ben-Dor G, Skews B, Sorek S (1993) Head-on collision of normal shock waves with rigid porous materials. Experiments in Fluids 15: 183–190

Levy A, Sorek S, Ben-Dor G, Bear J (1995) Evolution of the balance equations in saturated thermoelastic porous media following abrupt simultaneous changes in pressure and temperature. Transport in Porous Media 21: 241–268

Levy A, Ben-Dor G, Sorek S (1996a) Numerical investigation of the propagation of shock waves in rigid porous materials: development of the computer code and comparison with experimental results. 324: 163–179

Levy A, Sorek S, Ben-Dor G, Skews B (1996b) Waves propagation in saturated rigid porous media: analytical model and comparison with experimental results. Experiments in Fluids 17: 49–65

Levy A, Ben-Dor G, Sorek S (1997) Numerical investigation of the propagation of shock waves in rigid porous materials-solution of the Riemann problem. Int J of Numerical Methods for Heat & Fluid Flow (to appear)

Li H, Levy A, Ben-Dor G (1995) Analytical prediction of regular reflection over porous surfaces in pseudo-steady flows. J Fluid Mech 282: 219–232

Sorek S, Bear J, Ben-Dor G, Mazor G (1992) Shock waves in saturated thermoelastic porous media. Transport in Porous Media 9: 3–13

Sorek S, Krylov A, Levy A, Ben-Dor G (1996) Simple waves in saturated porous media. Part II: The nonisothermal case. Japan Society of Mech Eng Int J B 39: 299–304